Crystal structure of the NAD complex of human deoxyhypusine synthase: an enzyme with a ball-and-chain mechanism for blocking the active site

Der-Ing Liao[1†], Edith C Wolff[2], Myung Hee Park[2] and David R Davies[1*]

Background: Eukaryotic initiation factor 5A (eIF-5A) contains an unusual amino acid, hypusine [N$^{\varepsilon}$-(4-aminobutyl-2-hydroxy)lysine]. The first step in the post-translational formation of hypusine is catalysed by the enzyme deoxyhypusine synthase (DHS). The modified version of eIF-5A, and DHS, are required for eukaryotic cell proliferation. Knowledge of the three-dimensional structure of this key enzyme should permit the design of specific inhibitors that may be useful as anti-proliferative agents.

Results: The crystal structure of human DHS with bound NAD cofactor has been determined and refined at 2.2 Å resolution. The enzyme is a tetramer of four identical subunits arranged with 222 symmetry; each subunit contains a nucleotide-binding (or Rossmann) fold. The tetramer comprises two tightly associated dimers and contains four active sites, two in each dimer interface. The catalytic portion of each active site is located in one subunit while the NAD-binding site is located in the other. The entrance to the active-site cavity is blocked by a two-turn α helix, part of a third subunit, to which it is joined by an extended loop.

Conclusions: The active site of DHS is a cavity buried below the surface of the enzyme at the interface between two subunits. In the conformation observed here, the substrate-binding site is inaccessible and we propose that the reaction steps carried out by the enzyme must be accompanied by significant conformational changes, the least of which would be the displacement of the two-turn α helix.

Addresses: [1]Laboratory of Molecular Biology, NIDDK, NIH, Bethesda, MD 20892-0560, USA and [2]Oral and Pharyngeal Cancer Branch, NIDR, NIH, Bethesda, MD 20892-4340, USA.

[†]Present address: Dupont Central Research and Development E228/332, Wilmington, DE 19880-0228, USA.

*Corresponding author.
E-mail: david.davies@nih.gov

Key words: initiation factor 5A, NAD, spermidine, structure, subunit interactions

Received: **15 September 1997**
Revisions requested: **22 October 1997**
Revisions received: **10 November 1997**
Accepted: **12 November 1997**

Structure 15 January 1998, **6**:23–32
http://biomednet.com/elecref/0969212600600023

Introduction

The precursor eukaryotic initiation factor 5A (eIF-5A) undergoes an essential post-translational modification at a specific lysine residue. The modification occurs via a series of reactions which convert lysine to N$^{\varepsilon}$-(4-aminobutyl-2-hydroxy)lysine. Deoxyhypusine synthase (DHS) catalyzes the synthesis of N$^{\varepsilon}$-(4-aminobutyl)lysine (deoxyhypusine), the initial step in the conversion pathway (for reviews see [1,2]). The reaction involves a single lysine residue, Lys50, in only one protein, making hypusine biosynthesis one of the most specific protein modification reactions known to date [3]. This modification is essential for eukaryotic cell proliferation, although its exact mode of action is unclear. Inactivation of the two eIF-5A genes in yeast [4,5], or as shown recently the DHS gene [6,7], causes loss of viability by arresting cell proliferation. As the first enzyme in the modification pathway, DHS occupies a critical position, and its inhibition has potential for control of eukaryotic cell proliferation.

DHS, a single protein, catalyzes a multistep reaction (Figure 1) involving two substrates, spermidine and the eIF-5A precursor protein, and a cofactor, nicotinamide adenine dinucleotide (NAD) [8–10]. DHS is highly specific for each substrate. The reaction involves an enzyme–imine intermediate formed between the 4-aminobutyl moiety from spermidine and the ε-amino group of Lys329 in the human enzyme [10]. This intermediate is essential for the overall reaction [10,11]. Upon addition of the eIF-5A precursor the butylamine moiety from the enzyme–imine intermediate is transferred to Lys50 of the eIF-5A precursor and is reduced to form deoxyhypusine. The NADH formed in the first step of the reaction is used for the reduction required in the last step (ECW, unpublished data).

The amino acid sequence of DHS has been deduced from either cDNA or genomic DNA for human [12], yeast [13], *Neurospora crassa* [14] and *Methanococcus jannaschii* [15], and partial peptide sequences have been determined for the enzyme isolated from rat testis [9] and *Neurospora* [16]. There is significant sequence identity across these diverse species, especially in certain regions of the enzyme (overall 58% identity, 72% similarity for human versus yeast; 50% identity, 71% similarity for human versus *Methanococcus*). The native enzyme exists as a tetramer of four identical subunits of 40 kDa to 43 kDa, depending on the species [9,12–16]. The number of active sites per tetramer has not been characterized biochemically, nor has the stoichiometry of substrate binding.

Figure 1

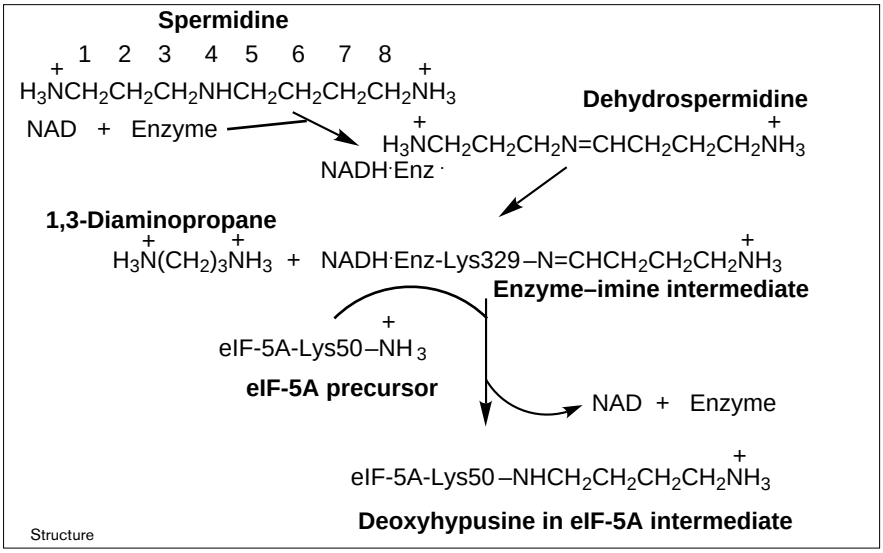

The reaction catalyzed by DHS. In the first step of the reaction, the NAD-dependent spermidine dehydrogenation between N4 and C5 generates NADH and dehydrospermidine. This step is followed by spermidine cleavage to yield 1,3-diaminopropane and an enzyme–imine intermediate [10]. In this intermediate the butylamine portion of spermidine is attached to the ε-amino group of Lys329 in the human enzyme via an imine linkage. In the final step, the butylamine moiety is transferred to the ε-amino group of Lys50 in the eIF-5A precursor protein, and the resulting eIF-5A–imine is reduced to form deoxyhypusine [8–10].

In earlier studies a large number of inhibitors structurally related to spermidine have been tested as probes for the spermidine-binding site [17]. Analogs of spermidine, for example closely related diamines such as 1,7-diaminoheptane (DAH; K_i = 5.6 μM) and its guanyl derivative 1-amino-7-guanidinoheptane (K_i = 0.01 μM) show competitive inhibition with respect to spermidine (K_m=7.2 μM). These compounds cause inhibition of hypusine formation, and arrest of proliferation in mammalian cells, including a variety of human cancer cell lines [18]. From a comparison of the inhibitory potency of these compounds for the enzyme *in vitro*, certain predictions were made regarding the structural features of the spermidine binding site [17].

We report here the refined crystal structure of human recombinant DHS in complex with NAD, crystallized in the presence of a known inhibitor, DAH. This structure reveals the nature of the active site and the positioning of the catalytic residues. However, density observed in the active site cannot easily be fitted by this inhibitor and may be the result of product binding.

Results and discussion

Overall structure of the DHS subunit and the assembly of the tetramer

DHS exists as a tetramer with four identical subunits related by 222 symmetry. This tetramer contains two pairs of tightly associated dimers, A1A2 and B1B2 (Figure 2), with two active sites, located in each dimer interface. Each active site has contributions from each of the two subunits, with one providing most of the catalytic residues and the other providing the binding site for the NAD.

Each subunit contains a central six-stranded parallel β sheet, a small antiparallel β sheet and 16 helices (Figures 3a,b).

Figure 2

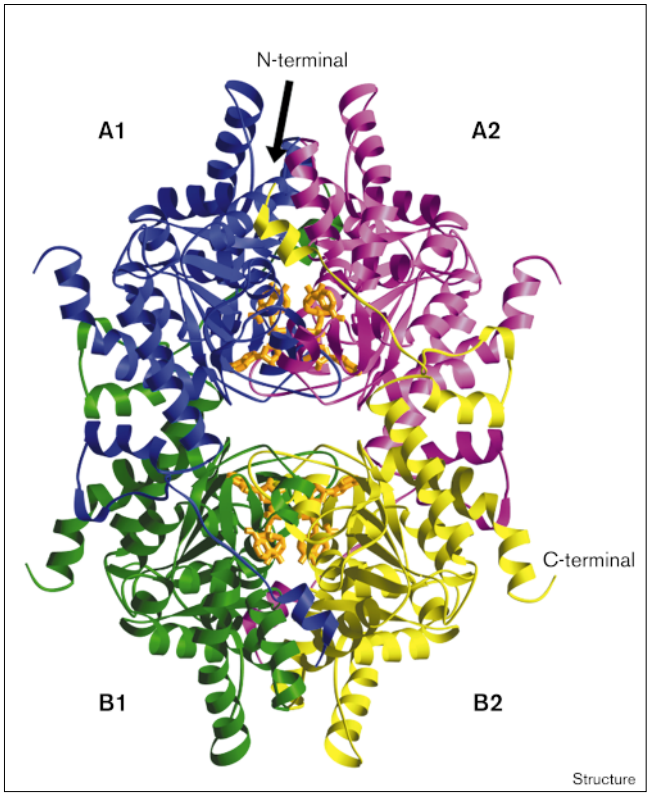

Ribbon drawing [38] of the DHS tetramer model with four bound NAD molecules (shown as orange stick models). The tetramer consists of two pairs of tightly associated dimers (i.e. dimer A, with A1 in blue and A2 in magenta; dimer B, with B1 in green and B2 in yellow). Two NAD molecules are bound in each dimer interface. The four subunits are related by 222 crystallographic symmetry.

Figure 3

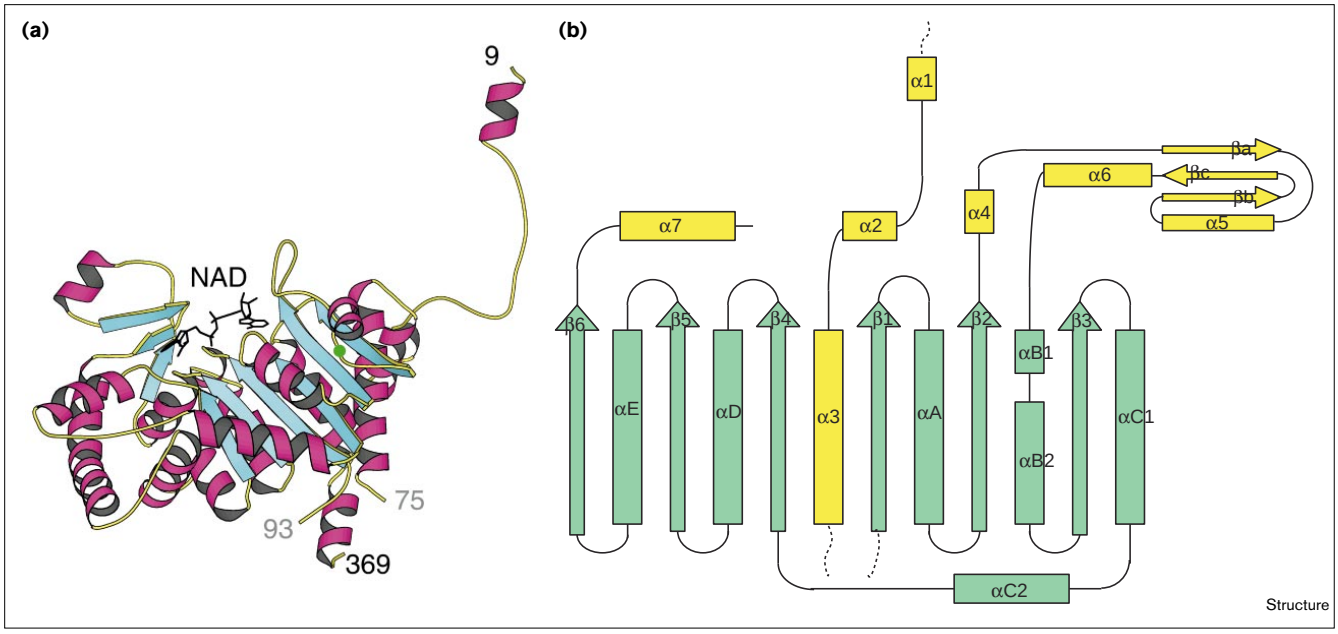

The topology of the DHS monomer. **(a)** Ribbon drawing [39] of the monomer of DHS with bound NAD (shown as a black stick model). The position of Lys329 is indicated as a light green circle. **(b)** Schematic diagram of the secondary structure. DHS contains a Rossmann fold [19] (shown in green) with insertions (in yellow) at the N and C termini and between the second β strand and the second α helix of the Rossmann fold. For a comparison with the secondary structures of other dehydrogenases see [20,21]. The β sheets that are part of the Rossmann fold are numbered sequentially from the N-terminal end (β1, β2, etc.), while those outside the fold are given lower case letters (βa, βb, βc); the α helices that are part of the Rossmann fold are indicated by capital letters (αA, βB, etc.) while those in the insertions are numbered (α1, α2, etc.). The starting and ending residues for each element are as follows: α1, 11–17; α2, 42–51; α3, 54–73; β1, 97–104; αA, 112–122; β2, 126–131; α4, 133–142; βa, 145–148; α5, 155–161; βb, 163–167; βc, 169–171; α6, 173–196; αB1, 203–214; αB2, 220–227; β3, 229–234; αC1, 240–250; αC2, 259–273; β4, 275–281; αD, 286–295; β5, 301–308; αE, 321–327; β6, 333–340; α7, 345–367. The dotted lines indicate disordered residues.

The overall fold of each subunit closely resembles the Rossmann dinucleotide binding motif [19] typical of most dehydrogenases [20], with insertions at three sites (indicated in yellow in Figure 3b). Near the N-terminal end of each monomer there is an insertion of some 35 residues which includes two helices, α2 and α3, with helix α3 packed parallel to the C-terminal helix α7. Between β2 and αC2 there is a cluster of helices (helices α4, α6 αB1, αB2 and αC1) packed on the edge of the parallel sheet on the opposite side from the N-terminal tail (Figure 3b). A three-stranded antiparallel β sheet (βa, βb and βc) and a short helix α5 are inserted between helix α4 and helix α6 of the cluster, located at the C-terminal end of the parallel sheet. One side of this small subdomain is part of the dimer interface that contains two active sites. The N-terminal tail is about 73 Å long (residues 9–39) with a two turn α helix at its end (residues 10–18).

The two closely interacting monomers form an extensive interface, with a buried area of 3221 Å^2 per monomer. The interaction of the two dimers to form a tetramer buries an additional 2599 Å^2 per monomer. In addition, the N-terminal tail from one monomer, for example B2 (yellow; Figure 2), extends across the side of the small subdomain of monomer A2 to the A1A2 interface where the short N-terminal end helix blocks the entrance to the active site in a ball-and-chain arrangement (Figure 4). The interaction of residues 9–25 with the other subunits buries an area of 948 Å^2. This interaction could play a major role in the control of enzyme activity as it is clear that in the form observed here this N-terminal helix would have to move in order to permit spermidine to enter the active-site cavity. A similar movement would be required for the penetration of the cavity by Lys50 of the eIF-5A precursor in order for the enzyme to carry out step 3 in Figure 1. In its present conformation the enzyme would be inactive, which is consistent with the pH profile of activity where maximum activity *in vitro* occurs at pH 9.2 and the activity at pH 4.5, where the crystallization occurred, is negligible.

The active site cavity

A striking feature of this enzyme is the buried nature of the active site (Figure 5). The site is accessed from the surface by a funnel about 16.4 Å long (measured from Cα17 of the N-terminal helix of B2 to the sidechain OH of Tyr305 of A1), which constricts to a narrow tunnel at a

Figure 4

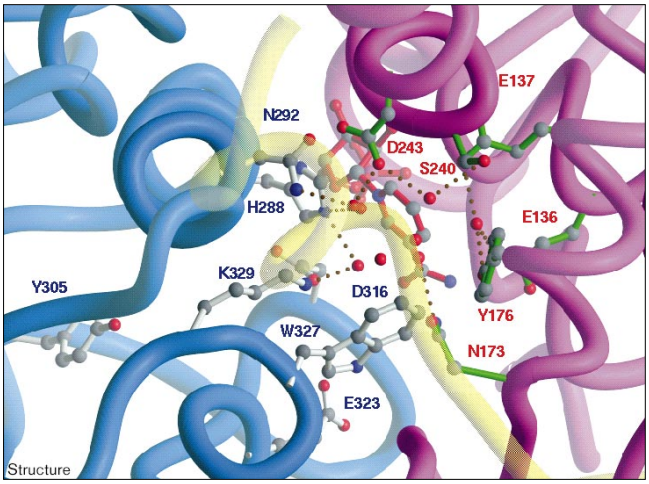

A ball-and-stick model of the DHS active-site structure. The N-terminal helix from a third monomer that covers the pocket entrance is in pale yellow. The orientation and color scheme of this figure are the same as in Figure 2. For clarity, only the nicotinamide ring and its adjacent ribose of NAD are shown. The hydrogen bonds between water molecules and sidechains of the protein residues are indicated by gray dotted lines; atoms are shown in standard colours. The N-terminal helix from the third monomer blocks the access to the active site.

level corresponding to the positions of the nicotinamide ring of NAD and the sidechain of Lys329, and then opens up into a long inner chamber. The shape of this active-site region immediately suggests the manner in which spermidine and the lysine sidechain of the eIF-5A precursor could interact with the enzyme during catalysis.

The NAD-binding sites run antiparallel to each other on the closely interacting pairs of subunits, related by the dyad axis (Figure 2). The adenosine ends of the two NAD molecules are fairly close to each other at the mid-level of the interface, with a distance of 2.69 Å between the two O3′ atoms. The nicotinamide ends of the two NADs, however, are separated by 22.9 Å at C4N, and the two Lys329 residues by 27.5 Å at their terminal NH_2s. The entrances to the cavities containing the active sites reside on the top and bottom of the pair of subunits in Figure 2.

Each NAD molecule forms hydrogen bonds with nine residues on one monomer (e.g. A1) and three with the monomer on the other side of the dimer interface (e.g. A2). In addition, the NAD makes hydrogen bonds with four tightly bound water molecules (see Figure 6a). The adenine ring is sandwiched between the two subunits, where it forms hydrogen bonds to the sidechains of Asp342, Asn106 of the closely associated monomer and to the mainchain of Asp313 of the other monomer. The conformations of the two ribose groups and the pyrophosphate are fixed by an intricate hydrogen-bonding network consisting of sidechains of Thr308, Asp238, Thr131 and mainchains of Ser105, Gly283, Asp238 from the associated monomer,

Figure 5

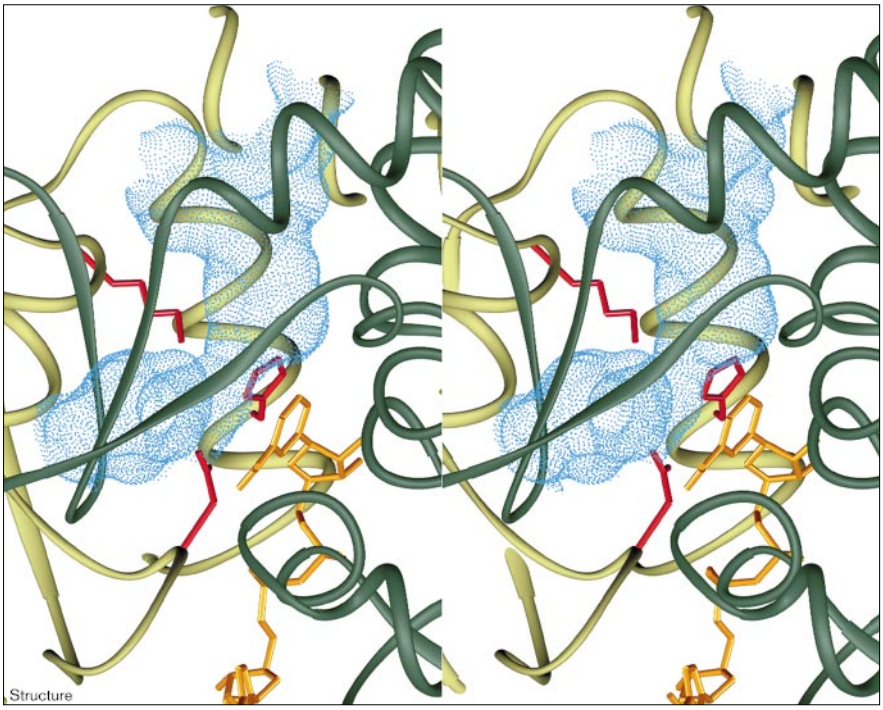

Stereoview of the dot surface of the active-site funnel [40]. The two subunits are colored light and dark green. Residues that are possibly involved in catalysis (Lys329, His288 and Asp243) are in red. The nicotinamide end of the NAD is in gold. The exit to the solvent is at the top of the figure. The dot surface defines the solvent-accessible cavity in the interior of the protein.

Figure 6

The details of NAD binding. **(a)** Schematic diagram of DHS–NAD interactions. Hydrogen bonds are shown as dashed lines. Most of the contacting residues come from one monomer (open boxes). The shaded residues come from the other closely associated monomer. **(b)** An omit $2F_o–F_c$ map of the NAD molecule contoured at the 1σ level. The NAD adopts a conformation that is only partly extended. The carboxamide group is rotated by about 23° from the plane of the nicotinamide ring, similar to that observed in crystals of lithium NAD [41] and in NAD bound to several dehydrogenases [20,21].

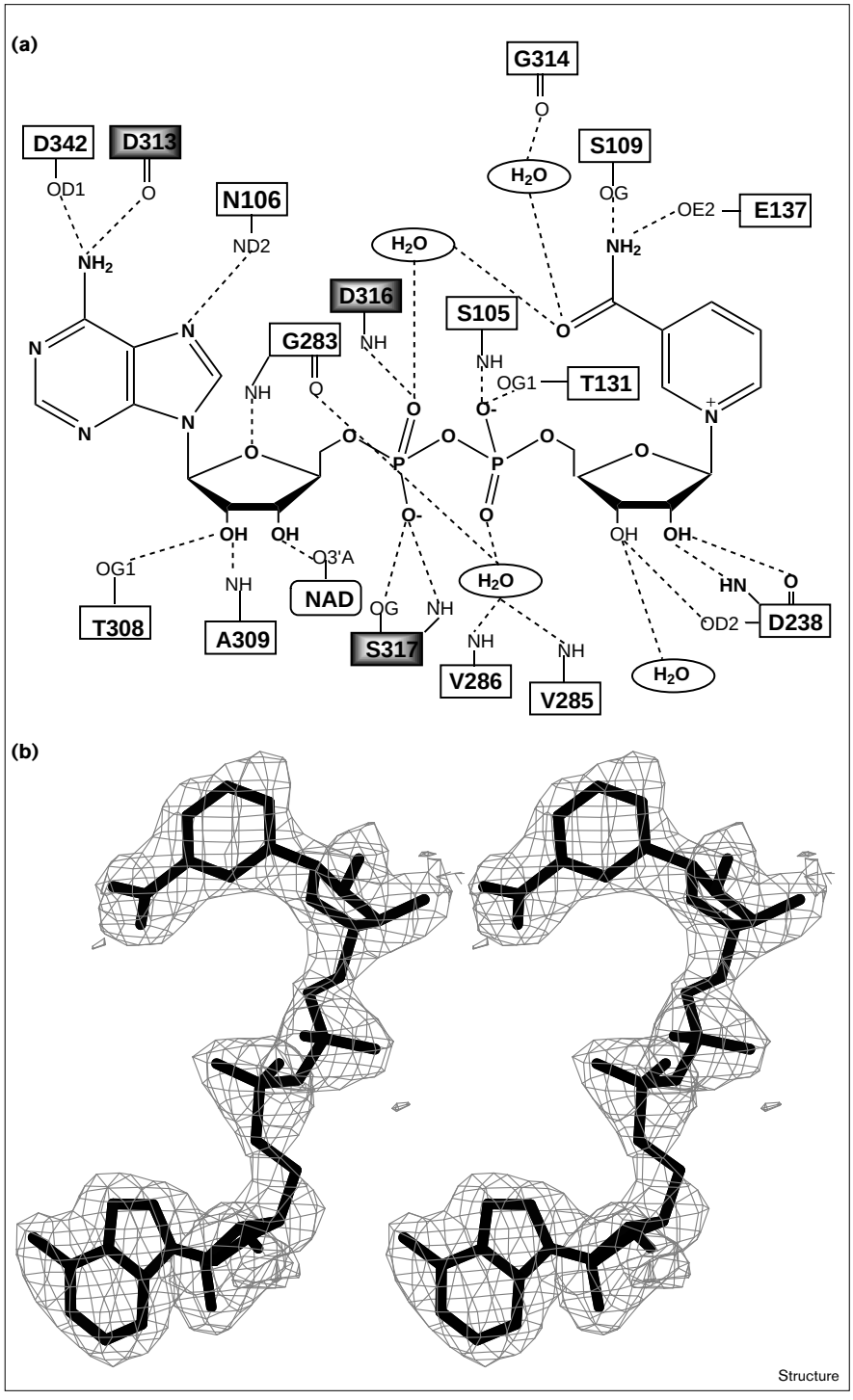

and the sidechain of Ser317 and the mainchains of Ser317, Asp316 from the other monomer. This network also involves three bound water molecules and the O3′A of the adjacent NAD. The amide nitrogen of the nicotinamide is hydrogen bonded to the sidechain of Ser109 and Glu137 of one monomer A1 and with two water molecules. One of the water molecules is associated with a phosphate group of the NAD. The nicotinamide ring has no interaction with the monomer across the dimer interface. There is a cavity ~ 5.5–7.0 Å wide and 9.5 Å long in the dimer interface, which is likely to be the spermidine-binding site. One side of the cavity contains the nicotinamide ring and the other

side contains several catalytically important residues (see below). The nicotinamide ring has the *syn* conformation relative to its ribose (Figure 6b). The A face of the ring is exposed to the solvent channel (Figure 5), consistent with the A stereospecificity previously determined for NAD in this reaction [8]. This orientation is in contrast to other well known dehydrogenases [21–23] which also have A specificity, but where the nicotinamide of the NAD is in the *anti* conformation. It should be noted that there are other exceptions to this correlation for which a rational explanation has been proposed [22].

As the NAD is tightly bound and completely buried in the dimer interface, it is likely that it stays in the enzyme for a complete cycle of reactions. This is consistent with the presumption that the same NAD molecule is used for the catalysis of the dehydrogenation, the first step of the reaction, and the reduction of the eIF-5A–imine intermediate, the last step of the reaction catalyzed by DHS. The hydride transfer for the reduction of the eIF-5A–imine intermediate should, therefore, take place near the region that has been proposed for the dehydrogenation of spermidine.

Model for spermidine binding

We have constructed a model of spermidine bound to the enzyme in the active-site cavity (Figure 7). The N4 and C5 of the spermidine are at the level of the Lys329 and the C4 of the nicotinamide ring of the NAD. The orientation of these groups enables the transfer of the hydride ion from C5 of the spermidine to the *re* face of the nicotinamide ring. Lys329 is positioned to attack the C5=N4 bond of dehydrospermidine in the first transimination reaction, which results in the formation of an enzyme–substrate intermediate, Enz–N=CH$(CH_2)_3NH_2$ [10]. In this model a number of surrounding amino acid residues form contacts with the spermidine and some could participate in the catalytic reaction. In particular, the conserved His288 is in the vicinity of the scissile bond and could act as the general base for the dehydrogenation reaction and be the proton donor for the subsequent imine transfer reaction. In the crystal structure, the Nz atom of Lys329 is only 3.65 Å from the NE2 of the histidine, and in addition, there is a water molecule that bridges both nitrogen atoms. The proximity of these two residues also suggests that the proton of the initial protonated imine, dehydrospermidine, might come from His288, which could have acquired a proton during the dehydrogenation reaction.

Figure 7

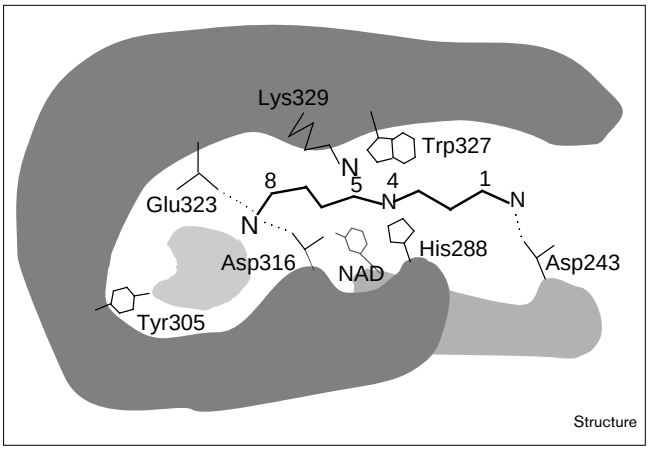

A proposed model of the spermidine-binding site of the enzyme showing the residues most likely to be involved. Asp243 and the principal binding area for NAD are located on the opposite monomer to that of the other binding residues. The funnel extends beyond the spermidine-binding area and includes the pocket which contains the unexplained density (shown here as a gray stippled area; see Figure 8). Potential hydrogen bonds are shown as dotted lines.

The OD2 of the conserved Asp316 is positioned only 4.3 Å from the NE2 of His288 and 4.8 Å from the Nz of Lys329. This atom may play a role in substrate binding, catalyzing the proton transfer from His288 to the dehydrospermidine and stabilizing a gem–diamine intermediate of the type proposed by Jencks [24] for the subsequent imine transfer reactions. The role of these residues in catalysis has been confirmed by ongoing site-directed mutagenesis studies (MHP and ECW, unpublished data).

According to this model, the amino group of the butylamine moiety of spermidine is anchored by Glu323 of one monomer, while NH2 at the propylamine end of spermidine can hydrogen bond to Asp243 of the other monomer. Trp327 is positioned to provide a hydrophobic interaction with the methylene groups of spermidine. There are some similarities between this model and the spermidine-binding site determined for a spermidine transporter, the only other spermidine-binding protein for which the crystal structure has been determined [25,26]. In the spermidine transporter protein the terminal amino groups of spermidine are anchored by acidic residues, while the methylene chain of spermidine is further fixed by hydrophobic interactions with up to four tryptophan residues.

Unexplained density in the interior pocket

DAH, a competitive inhibitor of the reaction at the optimal pH of 9.2, was present at approximately 5mM concentration in the crystallization solution. It was hoped that this inhibitor could be localized at the active site and would help define the mode of spermidine binding. However, no electron density was observed that could be interpreted as due to the DAH. Several small peaks of density in the active-site region can be readily interpreted as water molecules with one or more strong hydrogen bonds to the nearby residues (Figure 8). A continuous patch of electron density was found at the bottom of the inner pocket. This density has a length of about 6.4 Å,

Figure 8

Stereoview of the unexplained density in the interior pocket of the active site. F_o–F_c map contoured at the 4 standard deviation level.

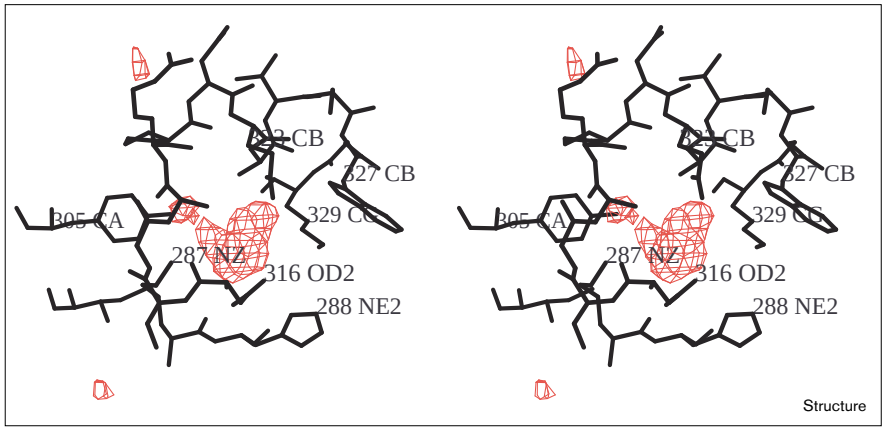

much shorter than the expected 10 Å for the nine atom DAH. No reasonable model of DAH can be fitted into this density and the contents of this binding pocket cannot be resolved directly by examination of this map. In addition, the density is 7 Å distant from the nicotinamide ring of NAD, being too far for hydride transfer between the substrate and the C4 atom of the nicotinamide. It is conceivable that this density represents a product derived from the 4-aminobutyl moiety of the enzyme–imine intermediate at Lys329, either in a cyclized form (1-pyrroline) [8] or as a straight-chain derivative, although these molecules do not provide a totally satisfactory fit to the observed density. The pocket could, however, conceivably be the binding site of the 4-aminobutyl moiety of the enzyme–imine intermediate at Lys329 during the reaction.

Possible eIF-5A precursor binding site

We have insufficient information here to propose specific roles for the active-site residues involved in the reaction between DHS and Lys50 of the eIF-5A precursor. The lysine residue from the eIF-5A precursor, however, must approach the Lys329–imine via the solvent channel seen in this structure. In the vicinity of the entrance to the active site there is a small hydrophobic patch, which in the structure reported here is covered by the small N-terminal helix originating from the other pair of dimers (see Figure 4). In order for either spermidine or the eIF-5A precursor to approach the active site, a conformational change must be induced such that the helix moves away to expose the active site to the substrates. The large area of the interface between the two subunits make it seem likely that the active-site channel will remain in more or less the same configuration. The presence of the hydrophobic patch at the entrance to the active site also suggests that hydrophobic interactions play an important role in the mechanism of protein–protein recognition between DHS and the eIF-5A precursor.

It is intriguing to speculate what controls access to the active site of DHS. A similar steric block of the active site of yeast glycogen phosphorylase by a long N-terminal arm is relieved by phosphorylation of a specific threonine residue [27]. In this case the phosphorylation may trigger a localized protein refolding that alters the dimer interface and results in activation. For DHS, however, there is no specific activating event that we are aware of, and the pH of the crystallization solution may have contributed to this inactive conformation and to the lack of binding of DAH. The presence of the precursor protein could induce a conformational change that would facilitate the reaction, but it cannot be essential as spermidine dehydrogenation and cleavage can be observed in its absence, albeit at a much slower rate than the complete reaction. Manipulation of the specific conditions of crystallization may afford insight into the enigma of the active conformation of DHS.

Biological implications

Deoxyhypusine synthase (DHS) catalyses the first step in the post-translational conversion of lysine to hypusine and in doing so plays a pivotal role in eukaryotic cell proliferation. The correlation of hypusine synthesis (which occurs only in the eukaryotic initiation factor, eIF-5A) and cell proliferation was first shown in human lymphocytes and other mammalian cells, but has also been demonstrated in cells depleted of spermidine (one of the substrates of DHS) by exposure to inhibitors of spermidine biosynthesis. In fact, an interesting corollary of this observation is the recognition that an important function of spermidine in supporting cell proliferation is its role as donor of the butylamine moiety of deoxyhypusine and hypusine [1,2]. The most convincing evidence for the vital role of mature eIF-5A, containing hypusine, derives from gene inactivation studies in the yeast *Saccharomyces cerevisiae*. Unless either one of the two eIF-5A genes is expressed, the

cells are not viable. Furthermore, disruption of the single gene for DHS, or inactivation of DHS activity also causes loss of cell viability. As both eIF-5A and DHS are highly conserved, and eIF-5A from different species is functionally interchangeable, it is reasonable to assume that eIF-5A performs a similar, fundamental function in cells throughout the eukaryotic kingdom, and that the presence of hypusine is equally critical for this function.

In spite of the clear evidence that eIF-5A is essential, its true cellular function has remained a mystery. Nevertheless, several roles have been postulated for this protein ([1,2] and references therein). As eIF-5A was initially isolated from ribosomes of rabbit reticulocyte lysates and showed activity in stimulating methionyl-puromycin synthesis (an *in vitro* assay for the first peptide bond formation), it was classified as a translation initiation factor [28]. A more recent eIF-5A depletion study, however, in which overall protein synthesis was only partially diminished, argues against a role for eIF-5A as a general protein synthesis factor [29]. Instead eIF-5A may promote the translation of a subset of mRNAs. In this regard, it is especially interesting that eIF-5A has been implicated as a cellular factor essential for Rev function in human immunodeficiency virus 1 (HIV-1) replication [30], and likewise for Rex function in human T cell leukemia virus (HTLV) replication [31]. Rev is presumed to be involved in the nuclear export of unspliced or partially spliced viral mRNAs that contain the Rev response element (RRE). It has been reported that certain dominant negative mutants of eIF-5A form a complex with Rev and RRE-containing RNA and inhibit HIV-1 replication in a human lymphocyte cell line [32]. It is possible, therefore, that a function of eIF-5A in normal cells is to facilitate the nuclear export and/or translation of certain specific mRNAs. Other lines of experiments suggest that eIF-5A may be involved in cell-cycle progression [1,2] (MHP, unpublished data).

Whatever the physiological function(s) of eIF-5A, all experiments have indicated that hypusine is an indispensable component of eIF-5A activity. Thus the enzymes that catalyse the formation of hypusine, DHS and deoxyhypusine hydroxylase, present unique targets for the manipulation of eIF-5A levels, and thereby of cell proliferation, through control of one specific reaction. The structure of the active site, as revealed in this study, helps to define the very strict specificity for the substrate spermidine, and structurally related inhibitors. This new information also lays the groundwork for the design of even more specific and effective inhibitors of DHS than those developed to date, inhibitors potentially useful in the therapy of hyperproliferative diseases or in the control of HIV-1 virus replication.

Materials and methods

Crystallization

Recombinant human DHS was overexpressed and purified as previously described [10,12], with additional steps of purification, involving successively, a hydroxyl apatite and butyl sepharose column. Single crystals of DHS were obtained at room temperature (~20°C) by vapor diffusion in hanging drops. The protein solution was prepared by mixing 50.0 µl of protein at 9.0 mg/ml, 3.0 µl of 0.1 M NAD and 3.0 µl of 0.1 M 1,7-diaminoheptane. The crystallization drops initially consisted of 1.0 µl of the protein solution and 1.0 µl of reservoir solution (1.7 M sodium/potassium phosphate and 100 mM HEPES, pH 7.0) resulting in a final pH of approximately 4.5. The drops were equilibrated against 1.0 ml of reservoir solutions and crystals were observed to grow to dimensions $0.15 \times 0.15 \times 0.4$ mm in 4–7 days. The crystals were transferred to a stabilizing solution containing 1.8 M sodium/potassium phosphate, 5 mM NAD, 5 mM 1,7-diaminoheptane, 100 mM HEPES (pH 7.5) and equilibrated for at least 8.0 h before being used for data collection and heavy-atom soaking experiments. The crystals are tetragonal, with space group $P42_12$, unit cell dimensions $a = b = 108.3$ Å, $c = 69.5$ Å, with one DHS monomer per asymmetric unit of the crystal, and a solvent content of 50% by volume. The crystals diffract to 2.2 Å resolution.

Structure determination

The structure was determined at 3.0 Å resolution by the single isomorphous replacement/anomalous (SIR/AS) difference method [33]. The X-ray diffraction data were collected at 95K on an RAXIS-II imaging plate system with CuKα X-rays from a Rigaku rotating-anode generator. Prior to data collection, both native and heavy-atom derivatized crystals were washed briefly in a solution containing 1.8 M sodium/potassium phosphate, 100 mM HEPES (pH 7.5) and 20% glycerol. The crystals were then mounted on nylon loops with a diameter of 0.1–0.3 mm and directly frozen in the 95K cold stream generated by an Oxford cryosystem. Diffraction data were collected at this temperature and were processed with the program DENZO [34]. The data statistics of the native data set and the mercury derivative data used for phase determination are listed in Table 1. The computer protein package PHASES [33] was used for heavy atom parameter refinement and SIR/AS difference phase calculation and solvent flattening. Only the centric reflections were used for the refinement of the heavy-atom parameters of the mercury derivative. The SIR phases derived from these parameters were then combined with the phase set generated by the anomalous difference of the same derivative. This generated a phase set with a mean figure of merit of 0.659. The final statistics of the crystallographic phase determination are summarized in Table 1. The 3.0 Å electron-density map calculated with these SIR/AS phases showed very clearly the solvent boundary and the secondary structure of the protein as well as some sidechain features. The connectivity of the map greatly improved after eight cycles of solvent flattening, assuming 45% solvent content, enabling the tracing of the polypeptide chain and sequence assignment. Electron density for the cofactor NAD could be clearly seen, but there was no clear density for the inhibitor. Neither NAD nor DAH were included in this initial model. Map interpretation and model building were effected using the program O [35]. The initial model contained 338 out of 369 residues.

Refinement

The initial structure was refined with X-PLOR [36], using 90% of the data between 6.0 and 2.2 Å for which $F > 2\sigma |F|$. A free R factor was calculated for the remaining 10% of the data at each refinement cycle to avoid over-fitting the data [37]. A total of seven cycles of refinement were carried out. Each cycle consists of simulated annealing using the slow-cooling protocol of X-PLOR, restrained individual B-factor refinement and manual model adjustment using the program O [35]. The NAD molecule was added to the model at the second cycle and six more residues at the C-terminal end of the molecule were included in the model at the fourth cycle of the refinement. Water molecules were incorporated into the model at cycles 2–7 by inspecting the F_o–F_c map contoured at 3σ after each cycle of the refinement.

Table 1

Crystallographic statistics.

Data set	Native DHS	DHS-Hg†
Resolution (Å)	2.2	2.7
Number of observations	108 771	57 432
Unique reflections	18 479	11 347
Completeness (%)*	86.1(41.9)	96.1(86.8)
R_{merge} (%)	7.4	11.8

*The figures in parentheses represent data for the final shell. $R_{iso} = 12.1\%$. †Number of binding sites for DHS-Hg = 3. $R_{centric} = 0.46$. Mean figure of merit = 0.608. Phasing power = 2.79 (single isomorphous replacement)/1.73 (anomalous). $R_{iso} = \Sigma \, ||F_h| - |F_n||$, where F_h and F_n are the heavy-atom and native structure factors, respectively. $R_{centric} = \Sigma \, ||F_h| - |F_n||$, where the sum is over the centric data.

Two regions of density in the $2F_o–F_c$ map could be identified in a pocket near the NAD molecules: one appears to be long enough for a five-atom single chain molecule such as 1,3-diaminopropane (DAP); the other is smaller and flattened and connects to the hydroxyl group of the sidechain of Tyr305. In an $F_o–F_c$ difference map, these two regions join to form one continuous patch of density (Figure 8). We have attempted to fit a DAH model into these two pieces of density causing the free R factor to decrease by 0.4% and the working R factor by 0.2%. However, the model still seems to be too large for the density. Alternatively, fitting the larger piece of density with a diaminopropane molecule and the small piece with a water molecule also lowered the free and working R factors by the same values. Residual density still remained, however, between the two pieces in the difference Fourier map and the shape of the small piece of density does not look like a water molecule. In addition, measurement by mass spectrometry showed no low molecular weight impurity in the DAH sample used for crystallization. We have therefore concluded that the present data do not permit the unambiguous assignment of the contents of the binding pocket.

There are two segments of the protein that appear to be too disordered to provide adequate electron density: the N-terminal eight residues of the protein, for which there is no interpretable density; and the region between residue 75 and 93 where the quality of the density is not sufficient for map interpretation. Also left uninterpreted were the two regions of density in the active-site pocket. The final model consists of 343 residues, 267 water molecules and one NAD molecule. The working R factor for this model is 15.3% and the free R factor is 24.2% for the 16,140 reflections used for the refinement. The rms deviations from ideal values for bond lengths and bond angles are 0.009 Å and 1.492. The average rms difference in B values is 1.44 Å^2 for 344 mainchain residues and 3.03 Å^2 for 287 sidechain residues. The mainchain tracing of the entire monomer is shown in Figure 9. The final $2F_o–F_c$ map of a region of the β sheet is included in the supplementary material available with the internet version of this paper.

Modeling of the DHS–spermidine complex

We have attempted to model a spermidine molecule within the active site of the enzyme based on two criteria: first, the C5 atom of the spermidine was located within hydrogen-bonding distance of the C4 atom of the nicotinamide ring of NAD to facilitate hydride transfer; second, the secondary nitrogen atom N4 of the spermidine should be within hydrogen-bonding distance of a general base, in this case His288, for proton transfer. The conformations of the spermidine and some sidechains of the nearby residues were manually adjusted to avoid unfavorable contacts, but the sidechain rearrangement was kept to a minimum. The model for spermidine was created using the program SYBYL and the manual modeling of the complexes was done using the computer graphic program O. No additional energy minimization for the model was performed.

Accession numbers

The atomic coordinates have been deposited in the Brookhaven PDB with accession number 1DHS.

Figure 9

Stereoview mainchain Cα trace of DHS. Every tenth residue and the N and C termini are labeled.

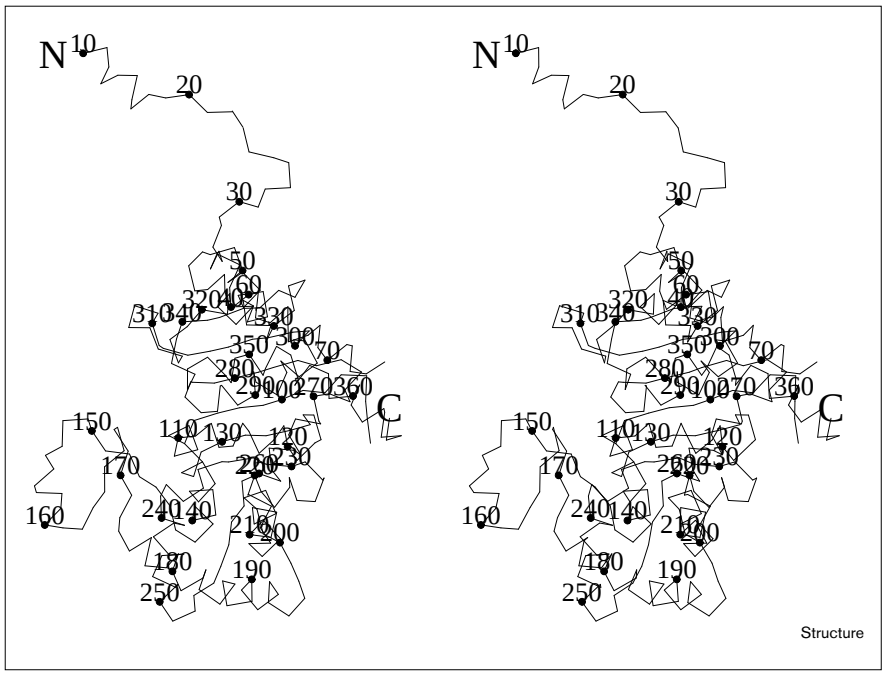

Supplementary material

Supplementary material available with the internet version of this paper contains the final $2F_o–F_c$ map for selected residues of DHS.

Acknowledgements

We thank Fred Dyda and Gerson Cohen for valuable assistance in the preparation of the figures and for stimulating discussions. We thank Douglas Jordan and Alan Rendina for mass spectrometry analysis of the inhibitor and protein samples and for many useful discussions.

References

1. Park, M.H., Wolff, E.C. & Folk, J.E. (1993). Is hypusine essential for eukaryotic cell proliferation? *Trends Biochem. Sci.* **18**, 475–479.
2. Park, M.H., Lee, Y.B. & Joe, Y.A. (1997). Hypusine is essential for eukaryotic cell proliferation. *Biol. Signals* **6**, 115–123.
3. Krishna, R.G, & Wold, F. (1993). Post-translational modification of proteins. *Adv. Enzymol. Relat. Areas Mol. Biol.* **67**, 265–298.
4. Schnier, J., Schwelberger, H., Smit-McBride, Z., Kang, H.A. & Hershey, J.W.B. (1991). Translation initiation factor 5A and its hypusine modification are essential for cell viability in yeast. *Mol. Cell Biol.* **11**, 3105–3114.
5. Wohl, T., Klier, H., Ammer, H., Lottspeich, F. & Magdolen, V. (1993). The HYP2 gene of *Saccharomyces cerevisiae* is essential for aerobic growth: characterization of different isoforms of the hypusine-containing protein Hyp2p and analysis of gene disruption mutants. *Mol. Gen. Genet.* **241**, 305–311.
6. Sasaki, K., Abid, M.R. & Miyazaki, M. (1996). Deoxyhypusine synthase gene is essential for cell viability in the yeast *Saccharomyces cerevisiae*. *FEBS Lett.* **384**, 151–154.
7. Park, M.H., Joe, Y.A. & Kang, K.R. (1997). Deoxyhypusine synthase activity is essential for cell viability in the yeast *Saccharomyces cerevisiae*. *J. Biol. Chem*., in press.
8. Wolff, E.C., Park, M.H. & Folk, J.E. (1990). Cleavage of spermidine as the first step in deoxyhypusine synthesis: the role of NAD. *J. Biol. Chem.* **265**, 4793–4799.
9. Wolff, E.C., Lee, Y.B., Chung, S.I., Folk, J.E. & Park, M.H. (1995). Deoxyhypusine synthase from rat testis: purification and characterization. *J. Biol. Chem.* **270**, 8660–8666.
10. Wolff, E.C., Folk, J.E. & Park, M.H. (1997). Enzyme–substrate intermediate formation at lysine 329 in human deoxyhypusine synthase *J. Biol.Chem.* **272**, 15865–15871.
11. Joe, Y.A., Wolff, E.C., Lee, Y.B. & Park, M.H. (1997). Enzyme–substrate intermediate at a specific lysine residue is required for deoxyhypusine synthesis: the role of Lys329 in human deoxyhypusine synthase. *J. Biol. Chem*., in press.
12. Joe, Y.A., Wolff, E.C. & Park, M.H. (1995). Cloning and expression of human deoxyhypusine synthase cDNA: structure-function studies with the recombinant enzyme and mutant proteins *J. Biol. Chem.* **270**, 22386–22392.
13. Kang, K.R., Wolff, E.C., Park, M.H., Folk, J.E. & Chung, S.I. (1995). Identification of *YHR068w* in *Saccharomyces cerevisiae*. Chromosome VIII as a gene for deoxyhypusine synthase: expression and characterization of the enzyme. *J. Biol. Chem.* **270**, 18408–18412.
14. Tao, Y. & Chen, K.Y. (1995). Molecular cloning and functional expression of *Neurospora* deoxyhypusine synthase cDNA and identification of yeast deoxyhypusine synthase cDNA. *J. Biol. Chem.* **270**, 23984–23987.
15. Bult, C., *et al.,* & Venter J.C. (1996). Complete genome sequence of the methanogenic Archaeon, *Methanococcus jannaschii*. *Science* **273**, 1058–1073.
16. Tao, Y. & Chen, K.Y. (1995). Purification of deoxyhypusine synthase from *Neurospora crassa* to homogeneity by substrate elution affinity chromatography. *J. Biol. Chem.* **270**, 383–386.
17. Jakus, J., Wolff, E.C., Park, M.H. & Folk, J.E. (1993). Features of the spermidine binding site of deoxyhypusine synthase as derived from inhibition studies: effective inhibition by bis- and mono-guanylated diamines and polyamines. *J. Biol. Chem.* **268**, 13151–13159.
18. Park, M.H., Wolff, E.C., Lee, Y.B. & Folk, J.E. (1994). Antiproliferative effects of inhibitors of deoxyhypusine synthase: inhibition of growth of CHO cells by guanyl diamines. *J. Biol. Chem.* **269**, 27827–27832.
19. Rossmann, M.G., Liljas, A., Branden, C.-I. & Banaszak, L.J. (1975). Evolutionary and structural relationships among dehydrogenases. In *The Enzymes*. (Boyer, P.D., ed), pp. 61–102, Academic Press, NY, USA.
20. Bell, C.E., Yeates, T.O. & Eisenberg, D. (1997). Unusual conformation of nicotinamide adenine dinucleotide (NAD) bound to diphtheria toxin: a comparison with NAD bound to the oxidoreductase enzymes. *Protein Sci.* **6**, 2084–2096.
21. Eklund, H., Samama, J.-P. & Jones, T.A. (1984). Crystallographic investigations of nicotinamide adenine dinucleotide binding to horse liver alcohol dehydrogenase. *Biochemistry* **23**, 5982–5996.
22. Almarsson, O. & Bruice, T.C. (1993). Evaluation of the factors influencing reactivity and stereospecificity in NAD(P)H dependent dehydrogenase enzymes. *J. Am. Chem. Soc.* **115**, 2125–2138.
23. Young, L. & Post, C.B. (1996). Catalysis by entropic guidance from enzymes. *Biochemistry* **35**, 15129–15133.
24. Hogg, J.L., Jencks, D.D. & Jencks, W.P. (1977). Catalysis of transiminations through trapping by acids and bases. *J. Am. Chem. Soc.* **99**, 4772–4778.
25. Sugiyama, S., Vassylyev, D.G., Matsushima, M., Kashiwagi, K., Igarashi, K. & Morikawa, K. (1996). Crystal structure of PotD, the primary receptor of the polyamine transport system in *Escherichia coli*. *J. Biol. Chem.* **271**, 9519–9525.
26. Kashiwagi, K., Pistocchi, R., Shibuya, S., Sugiyama, S., Morikawa, K. & Igarashi, K. (1996). Spermidine-preferential uptake system in *Escherichia coli*: identification of amino acids involved in polyamine binding to PotD protein. *J. Biol. Chem.* **271**, 12205–12208.
27. Lin, K., Rath, R.L., Shirleko, C.D., Fletterick, R.J. & Hwang, P.K. (1996). A protein phosphorylation switch at the conserved allosteric site in GP. *Science* **273**, 1539–1541.
28. Safer, B. (1989). Nomenclature of initiation, elongation and termination factors for translation in eukaryotes. Recommendations (1988) of the Nomenclature Committee of the International Union of Biochemistry (NC-IUB). *Eur. J. Biochem.* **186**, 1–3.
29. Kang, H.A. & Hershey, J.W.B. (1994). Effect of initiation factor eIF-5A depletion on protein synthesis and proliferation of *Saccharomyces cerevisiae*. *J. Biol. Chem.* **269**, 3934–3940.
30. Ruhl, M., *et al*., & Hauber, J. (1993). Eukaryotic initiation factor 5A is a cellular target of the human immunodeficiency virus type 1 Rev activation domain mediating trans-activation. *J. Cell. Biol.* **123**,1309–1320.
31. Katahira, J., Ishizaki, T., Sakai, H., Adachi, A., Yamamoto, K., Shida, H. (1995). Effects of translation initiation factor eIF-5A on the functioning of human T-cell leukemia virus type I Rex and human immunodeficiency virus Rev inhibited *trans* dominantly by a Rex mutant deficient in RNA binding. *J. Virol.* **69**, 3125–3133.
32. Bevec, D., *et al*., & Hauber, J. (1996). Inhibition of HIV-1 replication in lymphocytes by mutants of the Rev cofactor eIF-5A. *Science* **271**, 1858–1860.
33. Furey, W. & Swaminathan, S. (1990). 14th American Crystallographic Association Meeting, April 8–13, 1990, New Orleans, Abstr. PA33.
34. Otwinowski, Z. (1993). Oscillation data reduction program. In *Data collection and Processing*. (Sawyer, L., Isaccs, N. & Bailey, S., eds), pp. 56–62, SERC Daresbury Laboratory, Warrington, UK.
35. Jones, T.A., Zou, J.-Y., Cowan, S.W. & Kjeldgaard, M. (1991). Improved methods for building protein models in electron density maps and the location of errors in these models. *Acta Cryst. A* **47**, 110–119.
36. Brünger, A.T., Kuriyan, J. & Karplus, M. (1987). Crystallographic R factor refinement by molecular dynamics. *Science* **235**, 458–460.
37. Brünger, A.T. (1992). Free R value: a novel statistical quantity for assessing the accuracy of crystal structures. *Nature* **355**, 472–475.
38. Carson, M. (1991). Ribbons 2.0. *J. Appl. Cryst.* **24**, 958–961.
39. Kraulis, P.J. (1991). MOLSCRIPT: a program to produce both detailed and schematic plots of protein structures. *J. Appl. Cryst.* **24**, 946–950.
40. Connolly, N.L. (1983). Analytical molecular surface calculation. *J. Appl. Cryst.* **16**, 548–558.
41. Reddy, B.S., Saenger, W., Mühlegger, K. & Weimann, G. (1981). Crystal and molecular structure of the lithium salt of nicotinamide adenine dinucleotide dihydrate. *J. Am. Chem. Soc.* **103**, 907–914.

Supplementary material

Crystal structure of the NAD complex of human deoxyhypusine synthase: an enzyme with a ball-and-chain mechanism for blocking the active site

Der-Ing Liao[1†], Edith C Wolff[2], Myung Hee Park[2] and David R Davies[1*]

Structure 15 January 1998, **6**: 23–32

Figure S1

Final $2F_o–F_c$ map of residues (from left to right) 276–281 (β4), 103–98 (β1) and 130–126 (β2).

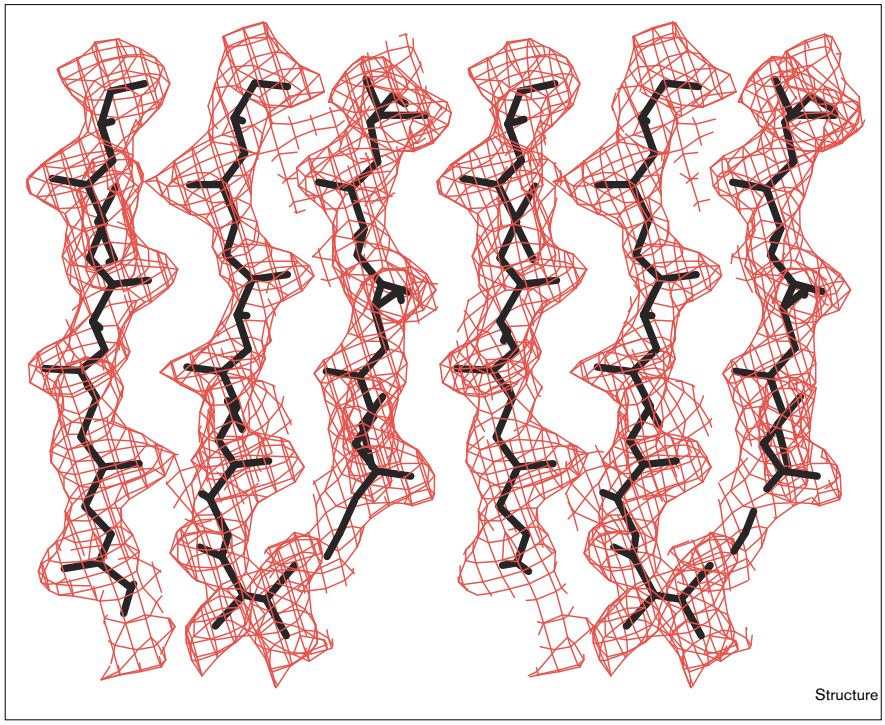

Table S2

Interdomain contacts (Å) in NiR-Pa.

N terminus-A–C domain-B							
8A	Glu	OE2	88B	Met	N	3.62	WH
8A	Glu	OE2	89B	Pro	N	3.54	WH
11A	Gln	CB	50B	Cys	SG	3.56	VW
15A	Ser	N	44B	Phe	O	3.05	H
19A	Pro	O	40B	Lys	NZ	2.79	H
22A	Val	O	40B	Lys	NZ	2.95	H
24A	Arg	CB	36B	Phe	CE1	3.60	VW
24A	Arg	NH2	31B	Met	O	3.39	WH
N terminus-A–D-domain-B							
6A	Ala	CB	422B	Gly	CA	3.48	VW
9A	Gln	CB	441B	Phe	CD1	3.69	VW
10A	Tyr	CD2	390B	Leu	CD1	3.43	VW
10A	Tyr	OH	327B	His	ND1	3.50	WH
10A	Tyr	OH	369B	His	NE2	2.84	H
14A	Ala	O	198B	Arg	NH1	3.01	H
15A	Ser	OG	223B	Glu	OE1	2.84	H
16A	Ala	N	223B	Glu	OE2	3.09	H
D domain-A–D domain-B							
261A	Lys	O	274B	Gln	NE2	3.44	WH
263A	Ile	CG2	269B	Met	CE	3.66	VW
267A	Arg	CD	276B	Tyr	CZ	3.69	VW
274A	Gln	NE2	261B	Lys	O	3.20	WH
274A	Gln	NE2	262B	Gln	OE1	3.56	WH
276A	Tyr	CZ	267B	Arg	CD	3.66	VW
315A	Leu	O	319B	Ser	N	2.90	H
316A	Thr	OG1	318B	Thr	OG1	2.83	H
316A	Thr	CG2	316B	Thr	CG2	3.62	VW
317A	Val	N	317B	Val	O	2.93	H
317A	Val	O	317B	Val	N	2.88	H
318A	Thr	OG1	316B	Thr	OG1	2.74	H
319A	Ser	N	315B	Leu	O	2.88	H
319A	Ser	O	315B	Leu	N	3.48	H
N terminus-A–C domain-A							
28A	Ala	N	69A	Gln	NE2	3.25	WH
C domain-A–D domain-A							
48A	Ala	O	281A	Arg	NH2	3.28	WH
49A	Gly	O	281A	Arg	NH2	2.93	H
53A	Val	N	279A	Glu	OE2	3.05	H
54A	Leu	N	279A	Glu	OE1	2.74	H
56A	Lys	O	277A	His	NE2	2.85	H

VW: van der Waals contacts, H: hydrogen bond, WH: weak hydrogen bond, I: ionic pair. Order is: residue name, type and atom name.

Table S3

Contacts (Å) of NiR-Pa c and d_1 hemes, and phosphate and chloride.

C heme-A							
51A	His	NE2	601A	HEC	Fe	2.09	
88A	Met	SD	601A	HEC	Fe	2.33	
63A	Leu	CD1	601A	HEC	CHB	3.56	VW
71A	Arg	NH2	601A	HEC	O1A	3.01	H
79A	Leu	CD2	601A	HEC	C2A	3.37	VW
84A	Thr	OG1	601A	HEC	O1D	2.73	H
89A	Pro	CD	601A	HEC	C3C	3.67	VW
8B	Glu	CA	601A	HEC	CBC	3.51	VW
D heme-A							
182A	His	NE2	602A	HED	Fe	2.00	
603A	HO^-	O	602A	HED	Fe	2.05	
156A	Arg	NE	602A	HED	O1C	2.96	H
185A	Arg	NH2	602A	HED	O1A	3.46	WH
198A	Arg	NH2	602A	HED	O2B	2.47	H
225A	Arg	NE	602A	HED	O2B	2.94	H
225A	Arg	NE	602A	HED	OMB	3.12	H
225A	Arg	NH2	602A	HED	O2B	3.30	WH
226A	Ser	OG	602A	HED	O2A	2.54	WH
245A	Tyr	OH	602A	HED	OMB	3.04	H
285A	Ile	N	602A	HED	O2A	3.39	WH
372A	Arg	NE	602A	HED	O2D	2.80	H
372A	Arg	NH2	602A	HED	O1D	3.08	H
425A	Phe	CE1	602A	HED	CBD	3.51	VW
483A	Gln	NE2	602A	HED	O1D	3.16	H
531A	Gly	CA	602A	HED	CMD	3.63	VW
533A	Phe	CE1	602A	HED	CGD	3.58	VW
10B	Tyr	CE1	602A	HED	CHC	3.34	VW
OH^- A							
603A	HO^-	O	602A	HED	Fe	2.05	H
603A	HO^-	O	10B	TYR	OH	2.61	H
Pi^-A							
335B	His	ND1	604A	PO_4	O3	3.29	H
323W	Wat	O	604A	PO_4	O2	3.06	H
540B	His	ND1	604A	PO_4	O2	2.81	H
134W	Wat	O	604A	PO_4	O2	2.60	H
Cl^-A							
265A	Ser	N	605A	ION	Cl	3.39	H
269B	Met	N	605A	ION	Cl	3.28	H

VW: van der Waals contacts, H: hydrogen bond, WH: weak hydrogen bond, I: ionic pair. Order is: residue name, type and atom name.